

## <sup>29</sup>Si MAS NMR systematics of calcic and sodic-calcic amphiboles

MARK D. WELCH,<sup>1</sup> SHUANGXI LIU,<sup>2</sup> AND JACEK KLINOWSKI<sup>2</sup>

<sup>1</sup>Department of Mineralogy, The Natural History Museum, London SW7 5BD, U.K.

<sup>2</sup>Department of Chemistry, University of Cambridge, Lensfield Road, Cambridge CB2 1EW, U.K.

### ABSTRACT

We report the compositional systematics of the <sup>29</sup>Si MAS NMR spectra of richterite, <sup>[Al](Na,K,Rb)<sub>1</sub>(Na,Ca,Sr)<sub>2</sub>Mg<sub>5</sub>Si<sub>8</sub>O<sub>22</sub>(OH,F)<sub>2</sub>; pargasite, NaCa<sub>2</sub>Mg<sub>4</sub>AlSi<sub>6</sub>Al<sub>2</sub>O<sub>22</sub>(OH)<sub>2</sub>; and fluor-edenite, NaCa<sub>2</sub>Mg<sub>3</sub>Si<sub>7</sub>AlO<sub>22</sub>F<sub>2</sub>. <sup>[Al]Na</sup> causes (1) splitting of T1 into two sites, while leaving T2 unsplit, and (2) the Q<sup>3</sup> chemical shift to be 2.5 to 3 ppm less negative than Q<sup>3</sup> when the A site is empty as in tremolite and magnesiohornblende. The preferential splitting of T1 is explained in terms of ordering of the A cation at *Am*. The effects of M4 and A-site chemistry upon the richterite spectra aid the assignment of peaks for pargasite and fluor-edenite. The long-range ordering of Al and Si over T1 and T2 sites in fluor-edenite synthesized at 2 kbar, and 1000 °C and pargasite synthesized at 1 kbar, and 930 °C has been calculated from their <sup>29</sup>Si MAS NMR spectra assuming that Al avoidance operates. The extent of long-range order is calculated from the intensities of the Q<sup>2</sup>(2Al), Q<sup>2</sup>(1Al), and Q<sup>2</sup>(0Al) peaks. An equation is derived that allows the extent of long-range Al-Si order to be calculated from <sup>29</sup>Si MAS NMR spectra of amphiboles. The spectrum of fluor-edenite is consistent with all <sup>[Al]Al</sup> being at T1 with maximal short-range disorder within the constraints of Al avoidance. The pargasite spectrum is more complex, because there is a probable peak coincidence of Q<sup>2</sup>(1Al) and Q<sup>3</sup>(2Al) at -82 ppm that must be considered. The presence of a Q<sup>3</sup>(0Al) peak in the pargasite spectrum indicates unambiguously that some long-range disorder exists, and this implies that Q<sup>3</sup>(2Al) groupings also occur. The calculated extent of long-range disorder in pargasite is 55 ± 10%. This value is consistent with the single-crystal X-ray data of Oberti et al. (1995a) for natural amphiboles extrapolated to <sup>[Al]Al</sup> = 2 apfu at 900 °C. The different long-range Al-Si ordering behavior of fluor-edenite and pargasite is explained in terms of the bond-valence requirements of O4. At high temperatures, configurational entropy becomes an important stabilizing factor, and structural distortion around O4 in pargasite and hornblende allows Al into T2, provided that O4 is coupled to Al at an adjacent M2 site, as in pargasite. The results for fluor-edenite, which has no <sup>[Al]Al</sup>, show that the low O4 bond-strength sum of the <sup>[Al]M<sup>2</sup>Mg<sup>M4</sup>Ca</sup> configuration cannot be accommodated by sufficient structural relaxation, even at 1000 °C. Coupling between Al at M2 and T2 is an important control on Al-Si long-range order-disorder.</sup>

### INTRODUCTION

An important goal of experimental mineralogy is to determine the validity of using synthetic analogues of chemically and structurally complex minerals to evaluate their crystal chemistry and phase relations. This goal is particularly significant for the amphiboles because of their microstructural and crystal-chemical complexities. Considerable progress has recently been made in elucidating long-range cation ordering in synthetic *C2/m* amphiboles, and their phase relations show systematic compositional behavior with respect to pressure and temperature that mirrors the behavior of natural amphiboles closely (Na et al. 1986; Welch 1987; Jenkins 1988; Pawley 1992; Welch and Graham 1992). Rietveld refinement of powder X-ray diffraction patterns have provided

reasonably well constrained site occupancies for M1, M2, and M3 sites for synthetic amphiboles with relatively simple compositions (Raudsepp et al. 1987; Della Ventura et al. 1993a, 1993b, and 1997). Infrared spectroscopy has provided valuable information about cation ordering at the M1, M3, and A sites (Raudsepp et al. 1987; Robert et al. 1989; Welch et al. 1994; Hawthorne et al. 1996a).

Al-Si ordering on tetrahedral sites in synthetic amphiboles has proven to be much more difficult to quantify. There are two aspects of tetrahedral ordering in amphiboles: (1) long-range order over T1 and T2 sites and (2) short-range order involving local charge balance and Al avoidance. Because X-ray scattering factors for Al and Si are very similar, X-ray diffraction gives information about Al-Si long-range order only from mean T-

O bond lengths for T1 and T2 sites. Single-crystal X-ray studies of synthetic amphiboles are usually not possible because of the fine grain sizes involved. Although Boschmann et al. (1994) and Oberti et al. (1995b) grew sufficiently big crystals of fluor-edenite and fluor-pargasite by slow cooling from melts, temperatures corresponding to the observed Al-Si distributions are not known. Jenkins and Hawthorne (1995) used Rietveld analysis of powder X-ray data to determine the long-range ordering of Ga and Si over tetrahedral sites in Ga-substituted fluor-tremolite-fluor-pargasite amphiboles,  $\text{Ca}_2\text{Mg}_5\text{Si}_8\text{O}_{22}\text{F}_2\text{-NaCa}_2\text{Mg}_4\text{Ga}(\text{Ga}_2\text{Si}_6)\text{O}_{22}\text{F}_2$  (synthesized at 3 kbar and 1000 °C); there was up to 50% long-range Ga-Si disorder. This study was possible because of the high scattering contrast between Ga and Si. Jenkins et al. (1997) used  $^{29}\text{Si}$  MAS NMR spectroscopy to study Al-Si order-disorder in aluminous tremolites related to tremolite by the Mg-tschermak's substitution  $^{61}\text{Al}^{[4]}\text{Al} = ^{61}\text{Mg}^{[4]}\text{Si}$ , with  $^{[4]}\text{Al}$  up to 1.0. The spectra suggested that these amphiboles have considerable long-range Al-Si disorder, although this was not quantified in detail.

Application of the bond-valence method (Brown and Shannon 1973; Brown 1981) to amphiboles (e.g., Hawthorne 1983, 1997) suggests that Al avoidance operates to avoid the low bond-valence sums (underbonding) of bridging Al-O-Al O atoms ( $\sim 1.5$  v.u.). The method has also been successfully applied to understanding long- and short-range ordering over the other cation sites in amphiboles (e.g., Hawthorne 1997). Thermodynamically, bond-valence effects are essentially enthalpic. However, it is conceivable that at high temperatures a burgeoning configurational entropy contribution to the free energy,  $-\text{TS}_{\text{cfg}}$ , arising from cation disorder becomes important, and the extent to which the amphibole structure can accommodate Al-Si long-range disorder at high temperatures is discussed in this paper.

In minerals as crystal-chemically complex as amphiboles, it is useful to investigate cation ordering by using several experimental methods to try to obtain a well-founded consensus. We have used  $^{29}\text{Si}$  MAS NMR to quantify the distribution of Al and Si over T1 and T2 sites. The technique is sensitive to the nearest-neighbor (NN) and next-nearest-neighbor (NNN) environments of Si nuclei and provides information on long-range and short-range order. However, although much information can be contained in a  $^{29}\text{Si}$  MAS NMR amphibole spectrum, separating the contributions of long-range and short-range order to the overall  $^{29}\text{Si}$  MAS NMR spectrum of an aluminous amphibole is difficult. To provide a basis for the interpretation of  $^{29}\text{Si}$  MAS NMR spectra of aluminous amphiboles, and to quantify long-range Al-Si order-disorder, this work attempts to (1) consider the possible Al-Si ordering schemes, (2) accurately determine relative peak intensities, and (3) recognize possible peak coincidences. This paper also reports the first NMR experiments on richteritic amphiboles,  $^{[A]}(\text{Na,K,Rb})_1(\text{Na,Ca,Sr})_2\text{Mg}_5\text{Si}_8\text{O}_{22}(\text{OH,F})_2$ , and examines the effects of different M4 and A-site chemistries upon

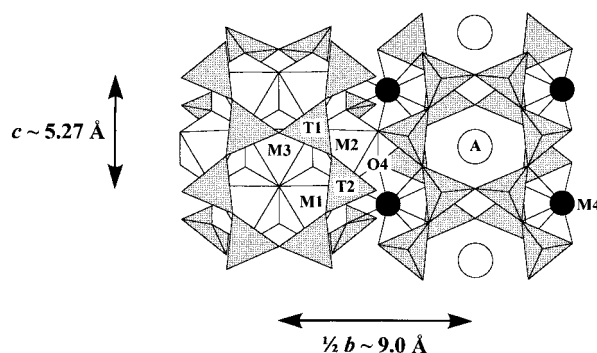


**FIGURE 1.** Part of the amphibole structure projected onto (100). In richterite and fluor-edenite, all the octahedral sites are occupied by Mg, whereas in pargasite one-fifth of the Mg is replaced by Al. T1 has three adjacent tetrahedra ( $Q^3$ ), T2 has two ( $Q^2$ ). Mean T1–O and T2–O bond lengths derived from X-ray diffraction studies indicate that Al is highly ordered onto T1. Only the  $A2/m$  position is shown for the A cation (see Fig. 5).

their  $^{29}\text{Si}$  MAS NMR spectra. These observations are then used to aid the interpretation of the  $^{29}\text{Si}$  MAS NMR spectra of fluor-edenite,  $\text{NaCa}_2\text{Mg}_5\text{Si}_7\text{AlO}_{22}\text{F}_2$ , and pargasite,  $\text{NaCa}_2\text{Mg}_4\text{AlSi}_6\text{Al}_2\text{O}_{22}(\text{OH})_2$ .

#### Long-range Al-Si order in pargasite and edenite

In the context of cation ordering, long-range order refers to the ordering of cations over crystallographically distinct sites. This study concerns the long-range ordering of Al and Si over T1 and T2 tetrahedral sites of the amphibole double chain (Fig. 1). X-ray studies indicate that  $^{[4]}\text{Al}$  is usually highly ordered at T1. This distribution has been explained as arising from the bonding requirements of the very underbonded O4 atom, which is bonded to T2, M2, and M4 cations (Fig. 1), so that a strong preference exists for a tetravalent element (Si) at T2 over a trivalent element (Al). Seven different NNN configurations are geometrically possible in amphiboles with  $^{[4]}\text{Al}$ : Using conventional NMR site notation these are T1 =  $Q^3(0\text{Al})$ ,  $Q^3(1\text{Al})$ ,  $Q^3(2\text{Al})$ ,  $Q^3(3\text{Al})$ , and T2 =  $Q^2(0\text{Al})$ ,  $Q^2(1\text{Al})$ ,  $Q^2(2\text{Al})$ . Here,  $Q^3(n\text{Al})$  refers to an Si at T1 with  $n$  Al NNNs and  $Q^2(n\text{Al})$  refers to an Si at T2 with  $n$  Al NNNs.

For future reference we define a long-range order parameter  $\Psi$ :

$$\Psi = 1 - \frac{2^{T2}\text{Al}}{^{[4]}\text{Al}} \quad (1)$$

where  $^{T2}\text{Al}$  is the number of Al atoms per formula unit (apfu) at T2 and  $^{[4]}\text{Al}$  is the number of tetrahedral Al apfu. The value of  $\Psi$  is one for complete order and zero for complete disorder. For fluor-edenite  $\Psi = 1 - 2^{T2}\text{Al}$ , and for pargasite  $\Psi = 1 - ^{T2}\text{Al}$ .

Local charge balance is known to be important in the short-range ordering of Al and Si in 2:1 and 2:1:1 layer silicates (Herrero et al. 1985, 1987; Circone et al. 1991; Welch et al. 1995) and may, therefore, also be important

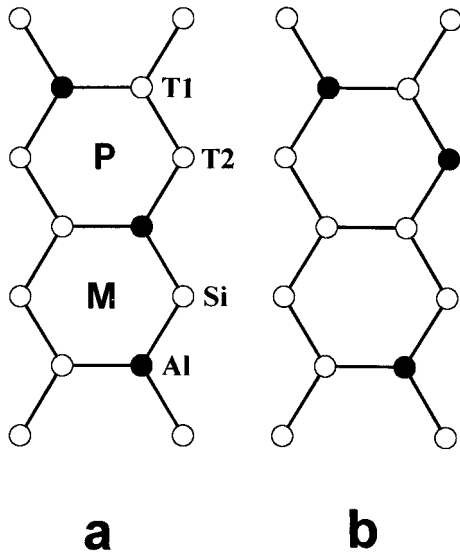


**FIGURE 2.** Al-Si order-disorder in pargasite when Al-O-Al avoidance operates. (a) All  $^{141}\text{Al}$  fully ordered onto T1 sites.  $\text{Q}^3(1\text{Al})$  and  $\text{Q}^2(1\text{Al})$  groupings predominate.  $\text{Q}^3(0\text{Al})$  groupings cannot arise in this completely long-range-ordered state. Examples of meta and para ring configurations (M and P) are indicated. (b) Long-range disorder in which some  $^{141}\text{Al}$  moves onto T2 sites. This produces  $\text{Q}^3(0\text{Al})$  and  $\text{Q}^3(2\text{Al})$  groupings (pairs).  $\text{Q}^3(3\text{Al})$  groupings result in considerable local charge imbalance. Note also that there is a net loss of one  $\text{Q}^3(1\text{Al})$  grouping.

in amphiboles. In pargasite, local charge balance with Al avoidance leads to an ordered state comprising only  $\text{Al}_2\text{Si}_4$  rings in which the two  $^{141}\text{Al}$  are in meta or para arrangements (Fig. 2). It is evident from Figure 2 that for such an ordered state any long-range Al-Si disorder imposed upon it must involve the creation of  $\text{Q}^3(0\text{Al})$  and  $\text{Q}^3(2\text{Al})$  pairs and arises from para rings:  $2 \text{Q}^3(1\text{Al}) = \text{Q}^3(0\text{Al}) + \text{Q}^3(2\text{Al})$ , where  $\text{Q}^3(2\text{Al}) = {}^{141}\text{Al} {}^{141}\text{Al} {}^{141}\text{Si}$ . For the unlikely case of a pure meta chain with all Al at T1 on one side of chain, long-range disordering is not possible without first forming para rings (because of Al avoidance). In pargasite, the fraction of total Si at T1 is 33% for complete long-range order and 50% for complete long-range disorder.

For AlSi, tetrahedral stoichiometry, as in edenite, four groupings are expected to be important in both the long-range-ordered and disordered states:  $\text{Q}^3(0\text{Al})$ ,  $\text{Q}^3(1\text{Al})$ ,  $\text{Q}^2(0\text{Al})$ , and  $\text{Q}^2(1\text{Al})$ . The smallest possible proportions of  $\text{Q}^3(0\text{Al})$  and  $\text{Q}^2(0\text{Al})$  groupings are both 29%, and so these groupings should be prominent components of the fluor-edenite spectrum. The grouping that is most sensitive to the extent of long-range order is  $\text{Q}^2(1\text{Al})$ , which ranges from 29% in the ordered state to 14% for complete disorder (this can be as low as 7% if Al clustering occurs, although this violates local charge balance).  $\text{Q}^3(2\text{Al})$  groupings can contribute a maximum of only 7% in the disordered state, although this is likely to be much lower. In fluor-edenite, the fraction of total Si at T1 is 43% for

complete long-range order and 50% for complete long-range disorder.

#### Calculation of long-range Al-Si ordering from $^{29}\text{Si}$ MAS NMR spectra

Bond valence arguments (e.g., Hawthorne 1983, 1997) point strongly to the operation of Al avoidance in amphiboles, primarily because of the prohibitively low resulting bond-strength sum (1.5 v.u.) of the oxygen in the Al-O-Al O bridge, even with small contributions from  $^{141}\text{Na}$  or  $^{141}\text{K}$ . The only exception to this “rule” is the very unusual hyper-calcic amphibole fluor-canilloite, ideally  $\text{CaCa}_2\text{Mg}_4\text{AlSi}_5\text{Al}_3\text{O}_{22}\text{F}_2$ , in which a significant bond-valence contribution from  $^{141}\text{Ca}$  to O7 allows  ${}^{141}\text{Al}$ -O- ${}^{141}\text{Al}$  linkages to form (Hawthorne et al. 1996b). Because fluor-edenite and pargasite have  $^{141}\text{Na}$  but no  $^{141}\text{Ca}$  they are very unlikely to have Al-O-Al tetrahedral linkages. When Al avoidance operates, the topology of the amphibole double-chain allows the extent of long-range disorder to be calculated from the observed intensities of the  $\text{Q}^2(2\text{Al})$  and  $\text{Q}^2(1\text{Al})$  or  $\text{Q}^2(0\text{Al})$  peaks. The calculation is shown below.

Some definitions:

$n$  is the number of Si atoms per formula unit

sumT2 = the sum of the relative intensities of  $\text{Q}^2(2\text{Al})$ ,  $\text{Q}^2(1\text{Al})$ , and  $\text{Q}^2(0\text{Al})$  NNN peaks

$$= \text{Q}^2(2\text{Al}) + \text{Q}^2(1\text{Al}) + \text{Q}^2(0\text{Al}) \quad (2a)$$

$$\begin{aligned} \text{T2s} &= \text{fraction of T2 sites occupied by Si} \\ &= 0.25n \text{ sumT2} \end{aligned} \quad (2b)$$

$$\begin{aligned} \text{T2a} &= \text{fraction of T2 sites occupied by Al} \\ &= 1 - \text{T2s} \end{aligned} \quad (2c)$$

$$\begin{aligned} \text{T1s} &= \text{fraction of T1 sites occupied by Si} \\ &= 0.25n[1 - \text{sumT2}] \end{aligned} \quad (2d)$$

$$\begin{aligned} \text{T1a} &= \text{fraction of T1 sites occupied by Al} \\ &= 1 - \text{T1s} \end{aligned} \quad (2e)$$

Mass balance gives:

$$\begin{aligned} \text{T1s} &= 0.5[2\text{T2a} + 0.25n \cdot \text{Q}^2(1\text{Al}) + 0.5n\text{Q}^2(0\text{Al})] \\ &= 0.25n[1 - \text{sumT2}] \end{aligned} \quad (3)$$

This analysis reflects the fact that (1) all Al at T2 has two Si NNNs (Al-O-Al avoidance), (2) the  $\text{Q}^2(2\text{Al})$  grouping does not have Si at T1, (3)  $\text{Q}^2(1\text{Al})$  and  $\text{Q}^2(0\text{Al})$  groupings have one and two Si NNNs at T1, respectively, and (4) each  ${}^{141}\text{Si}$  is shared by two T2 NNNs (hence the initial 0.5 multiplier).

Substituting for T2a (Eqs. 2b and 2c) into Equation 3 and solving for  $\text{Q}^2(0\text{Al})$  gives:

$$\text{Q}^2(0\text{Al}) = \frac{n[2 - \text{Q}^2(1\text{Al})] - 8}{2n} \quad (4)$$

This formula is applicable to all amphiboles. The site

populations are calculated from Equations 2b–2e. Clearly the  $Q^2(OAl)$  peak can be used to calculate the  $Q^2(1Al)$  peak intensity, and this allows a check on possible peak coincidences as shown later.

## EXPERIMENTAL DETAILS

### Synthesis

Six synthetic richterites,  $^{[Al]}(Na,K,Rb)_1(Na,Ca,Sr)_2Mg_3Si_8O_{22}(OH,F)_2$ , fluor-edenite,  $NaCa_2Mg_5Si_7AlO_{22}F_2$ , pargasite,  $NaCa_2Mg_4AlSi_6Al_2O_{22}(OH)_2$ , and a natural tremolite (Welch and Pawley 1991) were studied by  $^{29}Si$  MAS NMR spectroscopy. All syntheses used gels as starting materials and were prepared using the method of Hamilton and Henderson (1968). Richterites were synthesized at 1 kbar and 800 °C (3–5 d) and gave 98–99% yields of well-crystallized amphibole with very minor clinopyroxene impurity. The synthesis conditions required for pargasite and fluor-edenite are defined by the melting and dehydration curves at high temperatures and kinetic constraints imposed by the metastable growth and persistence of very tenacious sodium-phlogopite and diopside at temperatures below 900 °C. It is well known that the synthesis of end-member edenite,  $NaCa_2Mg_5Si_7AlO_{22}(OH)_2$ , free from significant amounts of diopside and sodium-phlogopite metastable impurities, has not been achieved (Graham and Navrotsky 1986; Na et al. 1986; Welch 1987; Graham et al. 1989). However, Graham and Navrotsky (1986) successfully synthesized a sample of pure fluor-edenite at 2 kbar and 1000 °C. This sample (0.35 g) was provided by C.M. Graham for use in the present study. Pargasite (1.3 g) was synthesized at 1 kbar and  $932 \pm 6$  °C. Details of sample characterization are described in Welch et al. (1994) and Graham and Navrotsky (1986). Optical microscopy indicated that the products of richterite and pargasite syntheses were, typically, at least 98% amphibole with trace amounts of diopside. Powder X-ray diffraction showed that all products were monophase amphibole. Typical sizes of the larger crystals were 1–5  $\mu m$  diameter by up to 35  $\mu m$  long for the richterites and 2–6  $\mu m$  diameter by 15–25  $\mu m$  for fluor-edenite and pargasite.

### Electron microprobe analysis

Amphibole powders were dispersed in quick-setting UV-epoxy and polished to a 0.25  $\mu m$  finish. Electron microprobe analysis (EMPA) was carried out using a Cameca SX50 probe at 15 kV, 10 nA, a 1–2  $\mu m$  spot size, and 20 s counting time. These conditions considerably reduced Na loss while retaining good counting statistics. Standards used were synthetic wollastonite ( $CaK\alpha$ ), corundum ( $AlK\alpha$ ), periclase ( $MgK\alpha$ ), New Idria jadeite ( $NaK\alpha$ ,  $SiK\alpha$ ), celestine ( $SrK\alpha$ ), KBr ( $KK\alpha$ ), and RbI ( $RbK\alpha$ ). Si and Rb correction factors taking into account overlapping  $SiK\alpha$  and  $RbK\alpha$  peaks were obtained by performing an independent check in which Si was analyzed on the RbI standard and Rb on a quartz standard. The fine-grained, often acicular, nature of the richterites resulted in some oxide totals being as low as 80%, because

of the electron beam also entering the epoxy. However, these were accepted provided that they calculated to amphibole stoichiometry; analysis totals ranged from 80–99%. This was a satisfactory pragmatic solution, given the high purity of the products. A similar policy was adopted by Jenkins et al. (1997).

### High-resolution transmission electron microscopy

Samples were dispersed onto carbon-coated holey copper grids from a suspension in alcohol and allowed to dry. High-resolution transmission electron microscope (HRTEM) observations were made at 200 kV with a JEOL 200CX microscope ( $\pm 30^\circ$  double tilt) using a 40  $\mu m$  objective aperture and a 70  $\mu m$  condenser aperture. All samples were beam-sensitive. These experimental conditions minimized beam damage while providing interpretable photographs. Microstructural purity was estimated by auditing 1500 tetrahedral chains per sample.

### Powder X-ray diffraction

With the exception of pargasite, lattice parameters were obtained using an Enraf-Nonius position-sensitive X-ray detector with  $CuK\alpha 1$  radiation and a Si monochromator. Data were collected in the range  $10$ – $90^\circ 2\theta$  for 1.5 h. Peaks had (FWHMs) of 0.16–0.18  $^\circ 2\theta$ . The non-linear response of the detector was modeled using an algorithm provided by the manufacturer (using GUF1 software by Enraf). Amphibole diffraction patterns were corrected against an internal NBS Si standard. Typically positions of 35 peaks were used in each cell refinement.

### $^{29}Si$ MAS NMR spectroscopy

All spectra were acquired on a Chemagnetics CXP-400 multinuclear spectrometer. The operating frequency for  $^{29}Si$  MAS NMR was 79.45 MHz and samples were spun in nitrogen at 4.0 kHz. These  $^{29}Si$  MAS NMR spectra of fluor-edenite and pargasite were collected using a  $30^\circ$  (2  $\mu s$ ) pulse and a 180 s pulse delay, whereas much shorter pulse delays were possible for richterites (80 s) and tremolite (30 s). Between 452 and 928 scans were made. It is clear from the nearly ideal  $Q^3:Q^2$  intensity ratios obtained for the richterites and tremolite that the pulse delays used were sufficiently long to avoid spin-lattice relaxation problems. For fluor-edenite and pargasite, a series of experiments was conducted in which pulse delays of 30, 80, 120, and 180 s were used; very little spectral difference was seen between 120 and 180 s delays, whereas shorter times resulted in noticeably different spectra. The presence of  $^{[Al]}$  apparently results in longer spin-lattice relaxation times for  $^{29}Si$  nuclei in amphiboles. These  $^1H$ - $^{29}Si$  CP/MAS experiments used a contact time of 10 ms, a  $90^\circ$  (4  $\mu s$ ) pulse, a 10 s pulse delay and 1884–4156 scans. The Hartmann-Hahn cross-polarization condition was set in one scan of a sample of high-quality kaolinite. Si chemical shifts are given in parts

TABLE 1. Chemical and crystallographic data for richterites, fluor-edenite, and pargasite

	K/Rb	Na	Sr	Ca	Mg	Al	Si	<i>a</i> (Å)	<i>b</i> (Å)	<i>c</i> (Å)	$\beta^\circ$	<i>V</i> (Å <sup>3</sup> )
Richterite	—	1.92(6)†	—	0.93(5)	5.08(8)	—	8.03(5)	9.902(4)†	17.987(9)	5.2721(2)	104.28(3)	910.0(10)
K-richterite	0.95(2)	1.00(3)	—	0.93(7)	5.06(8)	—	8.06(6)	10.027(5)	18.018(10)	5.2660(4)	104.61(3)	920.1(15)
Fluor-K-richterite	0.92(3)	0.99(3)	—	1.07(2)	4.93(7)	—	7.95(9)	9.984(4)	17.979(8)	5.2778(5)	104.91(1)	915.9(9)
Sr-richterite	—	2.02(6)	0.95(4)	—	4.98(5)	—	8.00(6)	10.020(2)	18.119(9)	5.2645(5)	104.98(1)	923.3(8)
Sr-K-richterite	0.96(3)	1.08(4)	1.00(7)	—	4.96(8)	—	8.02(4)	10.121(6)	18.138(11)	5.2740(8)	105.74(3)	930.6(12)
Rb-richterite	0.92(6)	1.04(5)	—	1.06(7)	4.93(6)	—	8.01(6)	10.067(4)	18.003(14)	5.2693(3)	104.86(2)	923.7(10)
Fluor-edenite*	—	1.06	—	1.91	5.05	1.00	7.00	9.857(3)	18.011(5)	5.2739(18)	104.86(2)	905.0(3)
Pargasite	—	1.03(3) <sup>+</sup>	—	1.94(3)	3.97(5)	2.95(4)	6.04(4)	9.905(2)	17.943(3)	5.281(1)	105.58(1)	904.0(3)

\*Data from Graham and Navrotsky (1986); formula recalculated from their microprobe analyses.

†Values in brackets are 1  $\sigma$  of the average values for microprobe and unit-cell data and refer to the last one or two decimal places.

per million from tetramethylsilane (TMS). Sample sizes were 0.3–1.3 g. Simulations of the <sup>29</sup>Si MAS NMR spectra were done using the package Spinsight provided by Chemagnetics. The relative intensities of the <sup>29</sup>Si peaks were determined by fitting pure Gaussian or mixed Gaussian-Lorentzian line shapes to the observed spectra by using least-squares deconvolution. The program adjusted the peak positions and widths iteratively until the best fit to the experiment spectrum was obtained with the minimum number of peaks.

## RESULTS

### Synthesis products

Chemical and crystallographic data for the amphiboles are given in Table 1. All amphiboles have nearly ideal stoichiometries and were adequate for the purposes of this study. Rubidium-richterite and potassium-fluorrichterite have small amounts of Na replacing Rb and K at the A site (about 0.06 and 0.08 <sup>131</sup>Na apfu, respectively). Within the small analytical errors, pargasite and fluor-edenite have ideal tetrahedral compositions. HRTEM indicated that, with the exceptions of rubidium-richterite and fluor-edenite, the amphiboles have essentially no chain-multiplicity (polysomatic) or chain-arrangement (orthorhombic stacking) defects. Rubidium-richterite has occasional single-chain defects amounting to less than 1% of the microstructure. Single, triple, and higher-order chain-multiplicity defects amount to 3% of the microstructure of fluor-edenite. Lattice parameters agree well with those obtained by Robert et al. (1989) and Della Ventura and Robert (1990) for richterite and Welch et al. (1994) for pargasite. The fluor-edenite data are from Graham and Navrotsky (1986).

### <sup>29</sup>Si MAS NMR spectroscopy

**Richterites.** Because all richterites have only Si on tetrahedral sites, <sup>29</sup>Si peaks are referred to here for brevity as Q<sup>3</sup> and Q<sup>2</sup>, rather than Q<sup>3</sup>(0Al) and Q<sup>2</sup>(0Al). Thus, Q<sup>3</sup> corresponds to T1 and Q<sup>2</sup> to T2. The <sup>29</sup>Si MAS NMR spectra of all richterites examined in this study are shown in Figure 3 and chemical shifts, peak widths, and relative intensities are given in Table 2. Also included for comparison is the <sup>29</sup>Si MAS NMR spectrum of a natural end-member tremolite studied by Welch and Pawley (1991).

All spectra could be simulated very well using pure Gaussian line shapes. A small peak at –84.5 ppm (up to 4% intensity) in some spectra did not cross-polarize (<sup>1</sup>H-<sup>29</sup>Si), whereas all other peaks do. Consequently, we attribute this peak to the minor clinopyroxene impurity present in these samples. Another small peak at –91 to –92 ppm is present in the spectra of richterite, potassium-richterite, potassium-fluorrichterite and rubidium-richterite, and amounts to 1–3% of the total spectral intensity. The origin of this minor peak is dealt with in the Discussion section.

The most important observation is that, with the exception of strontium-richterite (for which the Q<sup>3</sup> and Q<sup>2</sup> peaks overlap considerably), the single Q<sup>3</sup> peak of tremolite at –92 ppm is split in the richterite spectrum into two peaks of equal intensity. The difference in  $\delta$  Q<sup>3</sup> for the two Q<sup>3</sup> peaks is largest (2.0 ppm) when A = Rb and smallest (1.2 ppm) for Na, indicating a correlation with the size of the A cation. The Q<sup>2</sup> peak is unsplit, and  $\delta$  Q<sup>2</sup> is independent of the type of A cation. For M4 = NaCa,  $\delta$  Q<sup>2</sup> = –86.7  $\pm$  0.3 ppm, –87.3 ppm for M4 = Ca<sub>2</sub> in tremolite, and –88.0 ppm for potassium-strontium-richterite where M4 = NaSr. The C2/m polymorph of the richteritic amphibole hydro-sodium-magnesiocumingtonite (HSMC), Na<sub>3</sub>Mg<sub>5</sub>Si<sub>8</sub>O<sub>21</sub>(OH)<sub>5</sub>, in which M4 = Na<sub>2</sub> and A = Na, has  $\delta$  Q<sup>2</sup> = –85.6 ppm, and  $\delta$  Q<sup>3</sup> = –89.2 ppm (Liu et al. 1996). Hence the overall trend is for  $\delta$  Q<sup>2</sup> to become more negative as the average M4 cation size increases from Na to Sr. In no case is the Q<sup>2</sup> peak split. The data for the richterites show that for each different M4 chemistry there is a well-defined ( $\delta \pm 0.5$  ppm) and characteristic  $\delta$  Q<sup>2</sup> value. In the spectra of rubidium-richterite and potassium-fluorrichterite the –89 ppm Q<sup>3</sup> peak is slightly more intense than its partner at –91 ppm. The probable reason for this difference is the presence of small amounts of Na replacing Rb or K in the A site (about 0.06 and 0.08 <sup>131</sup>Na apfu, respectively).

**Fluor-edenite and pargasite.** The <sup>29</sup>Si MAS NMR spectra of fluor-edenite and pargasite are shown in Figure 4a as is the tremolite spectrum for comparison. Chemical shifts, peak widths, and relative intensities are shown in Table 2. The fluor-edenite and pargasite spectra contain five peaks at (fluor-edenite/pargasite) –78.5/–78.7, –82.0/–82.1, –84.3/–84.4, –86.8/–86.1, and –89.5/–89.0 ppm. With the exception of the intense peak at –86.8/

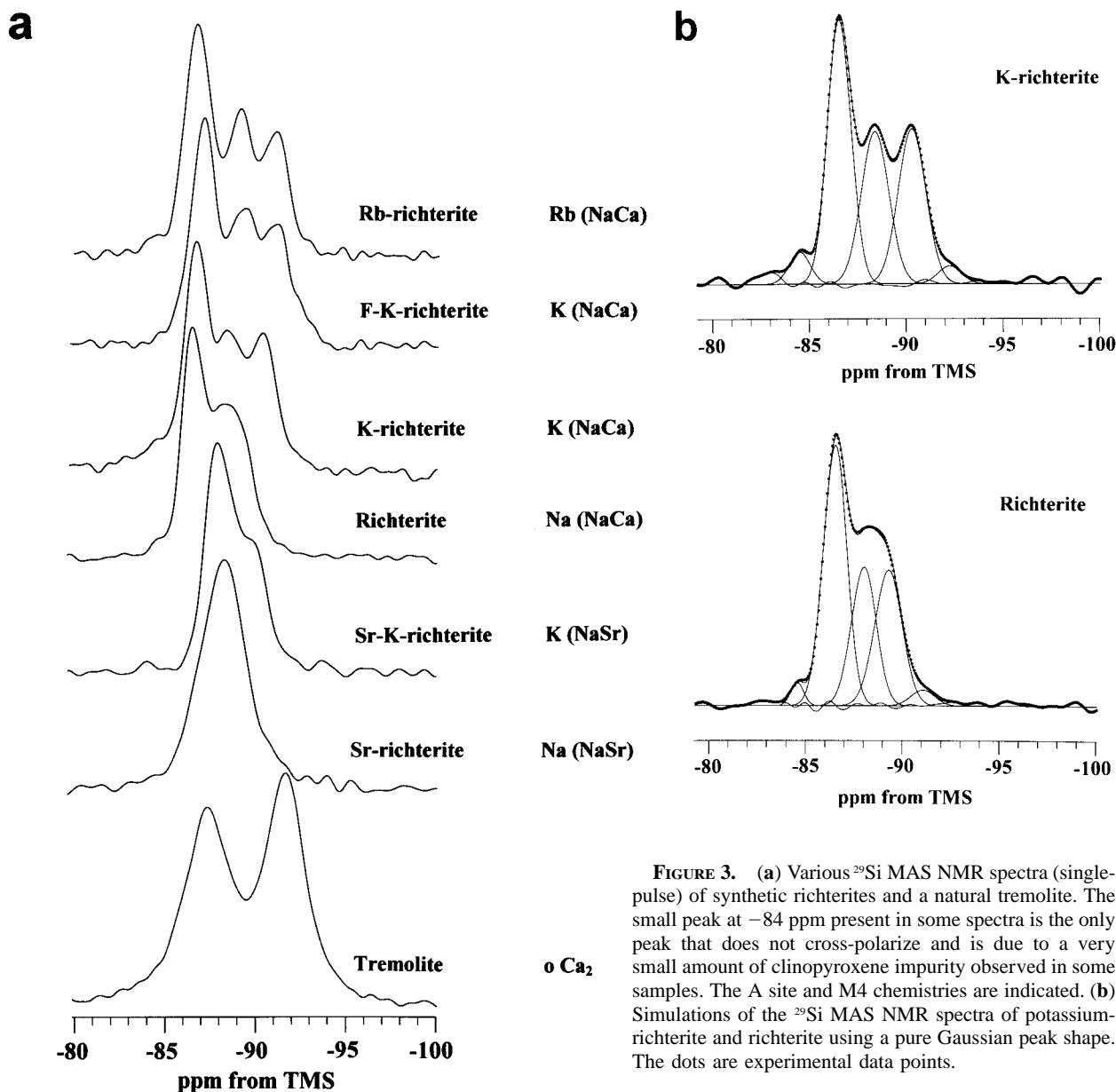


**FIGURE 3.** (a) Various  $^{29}\text{Si}$  MAS NMR spectra (single-pulse) of synthetic richterites and a natural tremolite. The small peak at  $-84$  ppm present in some spectra is the only peak that does not cross-polarize and is due to a very small amount of clinopyroxene impurity observed in some samples. The A site and M4 chemistries are indicated. (b) Simulations of the  $^{29}\text{Si}$  MAS NMR spectra of potassium-richterite and richterite using a pure Gaussian peak shape. The dots are experimental data points.

$-86.1$  ppm, the chemical shifts of respective peaks in the pargasite and fluor-edenite spectra agree to within  $0.5$  ppm. No splitting of  $\text{Q}^3$  peaks is apparent. Simulations of the pargasite and fluor-edenite spectra are shown in Figure 4b. Various mixtures of Gaussian and Lorentzian peak shapes were tested. Simulations using pure Gaussian and 75% Gaussian  $-25\%$  Lorentzian peak shapes gave excellent fits that were very similar to each other (Table 3). Increasing the amount of Lorentzian component beyond 25% worsened the fits, and a pure Lorentzian peak shape gave poor fits. The  $-82$  ppm peak is well resolved and easily simulated. Peak intensity data for fluor-edenite and pargasite are given in Table 3 along with ideal intensities for complete

long-range order and disorder. Absolute errors in the simulation of the  $-79$ ,  $-82$  and  $-87$  ppm peaks are about  $0.5$ ,  $1$ , and  $1\%$ , respectively. These peaks are the only ones used in the calculation of long-range order-disorder, and their errors are incorporated into the analysis.

## DISCUSSION

### Richterites

Two important observations pertain to the  $^{29}\text{Si}$  MAS NMR systematics of the richterites. (1) There are two equally intense  $\text{Q}^3$  peaks and one  $\text{Q}^2$  peak that have twice the intensity of each  $\text{Q}^3$  peak. (2)  $\delta \text{Q}^2$  depends upon M4 chemistry, becoming more negative as the average size

TABLE 2.  $^{29}\text{Si}$  peak data for amphiboles from this study

	$\delta$ (ppm)	Peak width (Hz)	Relative intensity (%)
Richterite	-84.5*	62	2
	-86.5	113	47
	-88.0	120	24
	-89.2	132	25
	-91.0†	115	2
K-richterite	-84.5*	101	4
	-86.5	113	45
	-88.4	132	24
	-90.3	132	24
	-92.2†	111	3
Fluor-K-richterite	-86.9	129	47
	-89.2	134	26
	-91.0	129	24
	-92.4†	85	3
	-84.2*	92	2
Rb-richterite	-86.6	140	49
	-89.0	135	27
	-91.0	126	24
	-92.8†	71	1
	-88.0	see table notes for comment	
Sr-richterite	-87.8	108	51
	-88.9	108	25
	-89.9	110	24
HSMC‡	-85.6	55	—
	-89.2	39	—
Tremolite	-87.3	244	49
	-91.7	203	51
	-82.0	140	22
Fluor-edenite	-78.5	136	1
	-82.0	140	22
	-84.3	124	14
	-86.8	186	34
	-89.4	217	28
Pargasite	-78.7	141	8
	-82.1	196	41
	-84.4	127	20
	-86.1	170	20
	-89.0	306	10

Notes: The reported data refer to simulations using a pure Gaussian lineshape. Absolute uncertainties on simulated peak intensities are about 1%. The spectrum of strontium-richterite has considerable peak overlap and it is not possible to obtain meaningful peak intensities in this case; the spectrum can be satisfactorily fitted with a single Gaussian peak at  $-88.0$  ppm and FWHM = 185 Hz.

\*Clinopyroxene impurity.

†Due to tremolite-like vacant A-site.

‡ $C2/m$  polymorph of hydro-sodian-magnesiocummingtonite (HSMC) from Liu et al. (1996).

of the M4 cation increases: NaSr is more negative than NaCa, which is less negative than Ca<sub>2</sub>. Q<sup>3</sup> peak splitting in the richterite spectra indicates that there are two distinct local A-T1 configurations. Both  $\delta$  Q<sup>3</sup> values are less negative than when the A site is empty, as in the case of tremolite ( $\delta$  Q<sup>3</sup> =  $-92$  ppm). The equal intensities of the two Q<sup>3</sup> peaks are reminiscent of the infrared spectrum of potassium-richterite observed by Robert et al. (1989) in which two absorptions of equal intensity occur at 3730 and 3735 cm<sup>-1</sup>, attributed to a split A site with K equally populating A2/m and Am sites. The richterite spectra of Robert et al. (1989) also contain a small peak at 3670 cm<sup>-1</sup>, which they ascribe to a tremolite-like (or magnesiocummingtonite-like) vacant A-site Mg<sub>3</sub>OH interaction. The latter may have its NMR counterpart in the small  $-91/-92$  ppm peak of the  $^{29}\text{Si}$  MAS NMR spectra of some richterites (Fig. 3). The tremolitic and magnesio-

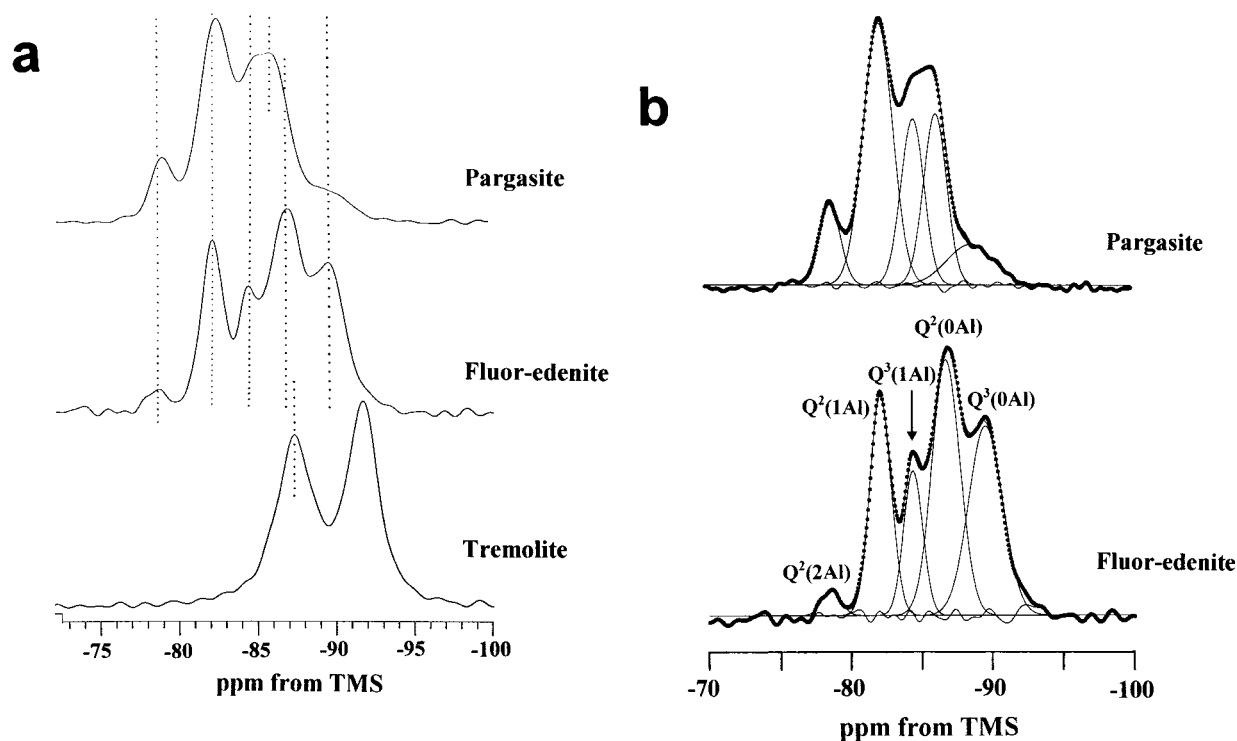
cummingtonitic peak amounts to only 1–3% of the total spectral intensity.

Figure 5 shows the environment of the A cation in  $C2/m$  amphiboles. The A-site cavity contains several subsites, corresponding to local potential-energy minima. These subsites are denoted A2/m, Am, and A2 and have multiplicities per A site of 1, 2, and 2, respectively. Single-crystal X-ray studies indicate that K is ordered at Am and Na is equally distributed over Am and A2. However, preferential splitting of T1 without T2 also splitting suggests that the local symmetry breaking involves retention of the mirror plane and loss of the diad; hence, the occupancy of Am is implied. Ordering at A2 or at a general position A1 would be expected to cause splitting of both T1 and T2. Consider K ordered onto the Am sites, lying within the mirror plane and displaced toward one of the two double chains bordering the A site. The other Am site is empty because there is only one A cation per A site. Hence there are two different local A-site configurations: <sup>Am</sup>K and <sup>Am</sup>□, where <sup>Am</sup>□ is a vacant Am site. The more negative peak of each pair of Q<sup>3</sup> peaks in the  $^{29}\text{Si}$  MAS NMR spectrum may reflect a situation in which one set of T1 sites sees what is in effect a “vacant” A site (compare with  $\delta$  Q<sup>3</sup> for tremolite at  $-92$  ppm), whereas the less negative peak may be due to T1 sites that see an occupied A site. For this to be so, the Am occupancy must be correlated between A sites, otherwise more than two different T1 sites occur. The extent of separation of the two Q<sup>3</sup> peaks may also correlate with the displacement from the A2/m position: The greater the displacement, the more distinct the full and empty Am sites are and the greater the separation of the peaks in the  $^{29}\text{Si}$  MAS NMR spectrum. This implies that Na is less displaced from A2/m than K and Rb. An unsplit Q<sup>3</sup> peak, as was found by Liu et al. (1996) for the  $C2/m$  polymorph of HSMC, implies that Na is at or close to A2/m.

#### Fluor-edenite and pargasite

In our interpretation of the NMR spectra of fluor-edenite and pargasite it is assumed that Al avoidance occurs, and so the extent of long-range Al-Si ordering is calculated using Equations 1 through 4. The tetrahedral stoichiometries of fluor-edenite (AlSi<sub>7</sub>) and pargasite (Al<sub>2</sub>Si<sub>6</sub>) allow some qualitative predictions to be made concerning the relative abundances of different Si NNN groupings, as discussed in the Introduction. For example, Q<sup>3</sup>(0Al) and Q<sup>2</sup>(0Al) groupings are expected to be much more common in edenite than in pargasite. The Q<sup>2</sup>(1Al) grouping should be important in both [a single Al at T1 creates two adjacent Q<sup>2</sup>(1Al) groups]. If local charge balance operates, so that excess charge is distributed as evenly as possible along the tetrahedral double chains (no Al clustering), then there should be no Q<sup>3</sup>(0Al) or Q<sup>3</sup>(3Al) groupings in fully ordered pargasite. Furthermore, any long-range disorder in pargasite creates Q<sup>3</sup>(2Al) and Q<sup>3</sup>(0Al) groupings (Fig. 2).

In a single-crystal X-ray study of fluor-edenite, Boschmann et al. (1994) found that Na was equally distributed



**FIGURE 4.** (a)  $^{29}\text{Si}$  MAS NMR spectra (single-pulse) of tremolite, fluor-edenite, and pargasite. Dotted lines indicate peak correlations among spectra. Peak assignments are discussed in the text. The  $\text{Q}^3(0\text{Al})$  peak occurs at  $-92$  ppm in tremolite and at  $-89$  ppm in fluor-edenite and pargasite. (b) Simulations of the fluor-edenite and pargasite spectra using a pure Gaussian peak shape. The dots are experimental data points. Peak assignments are shown for fluor-edenite.

over  $A_m$  and  $A_2$  sites. Hawthorne et al. (1996c) found that Na ordered completely at  $A_2$  in pargasite. However there are no indications of split T1 peaks in the  $^{29}\text{Si}$  MAS NMR spectra of fluor-edenite or pargasite. The richterite spectrum (Fig. 3) shows a relatively small splitting (1.2 ppm) that may point to a small displacement from  $A_2/m$ . It is possible that the displacements of Na from  $A_2/m$  to  $A_m$  or  $A_2$  sites in fluor-edenite and pargasite are too small to be detected by  $^{29}\text{Si}$  MAS NMR in these cases.

The  $-89.4$  ppm peak in the fluor-edenite spectrum is

due to  $\text{Q}^3(0\text{Al})$  because it has the most negative chemical shift, and this grouping is expected to be common in amphiboles with  $\text{AlSi}_7$  tetrahedral chemistry. This peak is 2.3 ppm less negative than the  $\text{Q}^3(0\text{Al})$  peak of tremolite ( $-91.7$  ppm). Jenkins et al. (1997) studied magnesiohornblende,  $\text{Ca}_2\text{Mg}_4\text{AlSi}_7\text{AlO}_{22}(\text{OH})_2$  (empty A site), by  $^{29}\text{Si}$  MAS NMR and found that  $\delta \text{Q}^3(0\text{Al})$  ( $-92.5$  ppm) is unaffected by the presence of  $^{141}\text{Al}$ . This suggests that the different  $\delta \text{Q}^3(0\text{Al})$  values of tremolite and fluor-edenite/pargasite are due to the presence of  $^{141}\text{Na}$  in the lat-

**TABLE 3.** Peak intensity data for fluor-edenite and pargasite obtained using pure Gaussian or 75% Gaussian and 25% Lorentzian peak shapes

	$\text{Q}^2(\text{nAl})$			3A1	$\text{Q}^3(\text{nAl})$			Calculations		
	2Al ( $-79$ ppm)	1Al ( $-82$ ppm)	0Al ( $-86/-87$ ppm)		2Al ( $-83$ ppm)‡	1Al ( $-84.5$ ppm)	0Al ( $-89$ ppm)	sum $\text{Q}^3$	$\text{Q}^2(0\text{Al})$ §	$\text{Q}^2(1\text{Al})$ §
Fluor-edenite ( $\Psi = 1$ )	1(2)*	22(22)	34(33)	0	0(0)	14(13)	28(29)	42(42)	32(32)	18(20)
( $\Psi = 0$ )	3	21	32	0	0	14	29	43		
Pargasite (5 peaks)	1	12	37	0	2	17	31	50		
6 peaks†	8(9)	41(41)	20(21)	0	?	20(20)	10(8)	30(28)	13(13)	27(25)
( $\Psi = 1$ )	8(9)	31(30)	20(21)	0	10(11)	20(20)	10(8)	40(39)	18(18)	27(25)
( $\Psi = 0$ )	17	33	17	0	0	33	0	33		
	4	20	24	5	8	26	11	50		

\*Values in brackets were obtained using a 75% Gaussian and 25% Lorentzian peak shape.

†Treats the  $-82$  ppm peak as an unresolved pair of  $\text{Q}^2(1\text{Al})$  and  $\text{Q}^2(2\text{Al})$  peaks at  $-81.7$  ppm and  $-83.1$  ppm, respectively.

‡Chemical shifts refer to six-peak simulation.

§Calculated using Equation 4.

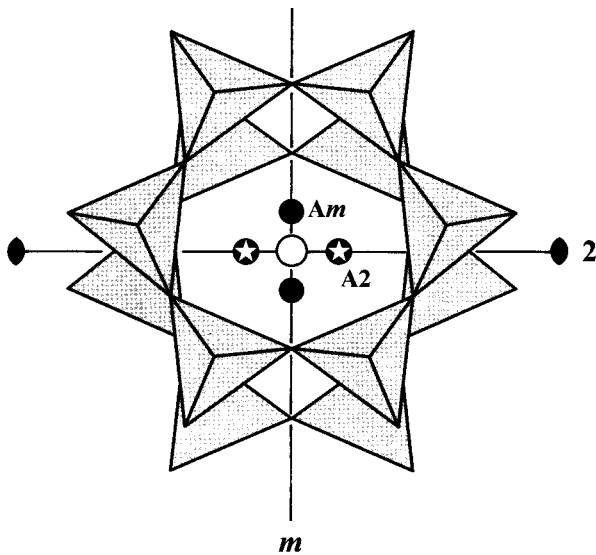


FIGURE 5. The environment of the amphibole A site showing the positions of Am and A2. The central position at A2/m lies at the intersection of the diad and mirror plane.

ter. It was noted above, with reference to the  $^{29}\text{Si}$  MAS NMR spectra of richterite and HSMC, that  $^{1\text{A}}\text{Na}$  shifts  $\delta$   $\text{Q}^3(0\text{Al})$  downfield by about 3 ppm to  $-88/-89$  ppm compared with an empty A site (e.g.,  $-92$  ppm in tremolite). The observed  $\delta$   $\text{Q}^3(0\text{Al})$  values of fluor-edenite ( $-89.4$  ppm) and pargasite ( $-89.0$  ppm) are compatible with this and an A site filled by Na. For magnesianhornblende tetrahedral chemistry, as for edenite, we expect at least four peaks from  $\text{Q}^3(0\text{Al})$ ,  $\text{Q}^3(1\text{Al})$ ,  $\text{Q}^2(0\text{Al})$ , and  $\text{Q}^2(1\text{Al})$  groupings, irrespective of the extent of long-range disorder. However, the  $^{29}\text{Si}$  MAS NMR spectrum of magnesianhornblende (in Jenkins et al. 1997 see Fig. 6, Amph 28-1) has only three peaks, at  $-83.4$ ,  $-87.6$ , and  $-92.5$  ppm with relative intensities of 10, 42, and 48%, respectively. The  $-92.5$  ppm peak corresponds closely to the position of the  $\text{Q}^3(0\text{Al})$  peak of tremolite. In view of the likely importance of  $\text{Q}^3(1\text{Al})$  groupings in magnesianhornblende, Jenkins et al. (1997) acknowledged that the  $-87.6$  ppm peak or, possibly, the  $-92.5$  ppm peak could be an unresolved pair of  $\text{Q}^2(0\text{Al})$  and  $\text{Q}^3(1\text{Al})$  peaks. In phlogopites and chlorites  $\delta$   $\text{Q}^3(1\text{Al})$  is consistently about 4 ppm less negative than  $\delta$   $\text{Q}^3(0\text{Al})$  (Circone et al. 1991; Welch et al. 1995). The  $\text{Q}^3(0\text{Al})$  and  $\text{Q}^3(1\text{Al})$  chemical shifts in these sheet-silicates occur at  $-91$  ppm and  $-87$  ppm, respectively. The sheet-silicate  $^{29}\text{Si}$  chemical shifts imply that the  $\text{Q}^2(0\text{Al})/\text{Q}^3(1\text{Al})$  peak coincidence in the magnesianhornblende spectrum is associated with the  $-88$  ppm peak. Does such a  $\text{Q}^3(1\text{Al})/\text{Q}^2(0\text{Al})$  peak coincidence occur in the spectra of pargasite and fluor-edenite? The richterite spectra indicate that  $^{1\text{A}}\text{Na}$  causes  $\delta$   $\text{Q}^3(0\text{Al})$  to become less negative by 2.5 ppm compared with when the A site is empty, whereas  $\delta$   $\text{Q}^2$  is unaffected by the presence of an A-site cation. A similar displacement of the  $\text{Q}^3(1\text{Al})$  peak from  $-87$  ppm results in  $\delta$   $\text{Q}^3(1\text{Al})$  of

around  $-84.5$  ppm. On this basis, we interpret the peak at  $-84.5$  ppm in the fluor-edenite spectrum to be due to  $\text{Q}^3(1\text{Al})$ . Thus, the observed relative peak intensities of fluor-edenite are:  $\text{Q}^2(2\text{Al}) = 1\%$ ,  $\text{Q}^2(1\text{Al}) = 22\%$ ,  $\text{Q}^2(0\text{Al}) = 34\%$ ,  $\text{Q}^3(1\text{Al}) = 14\%$ , and  $\text{Q}^3(0\text{Al}) = 28\%$ . The calculated intensity for  $\text{Q}^2(0\text{Al})$  of 32% confirms the assignment of the  $-87$  ppm peak to this grouping [recall that the richterite spectra indicate that  $\delta$   $\text{Q}^2(0\text{Al})$  is essentially constant for a particular M4 chemistry]. Table 3 shows that the observed peak intensities agree very well with an Al-Si ordering scheme in which there is complete long-range ordering of Al onto T1 with maximal short-range disorder for the constraint of Al avoidance. The  $\text{Q}^3$  sum of 42% is also consistent with complete ordering of Al at T1 (Table 3).

The case of pargasite is more complex. Four of the five resolved peaks ( $-78.7$  ppm,  $-82.1$  ppm,  $-84.4$  ppm, and  $-89.0$  ppm) have very similar chemical shifts in the fluor-edenite and pargasite spectra. The remaining peak occurs at  $-86.1$  ppm in the pargasite spectrum and at  $-86.8$  ppm in the fluor-edenite spectrum, where it is ascribed to  $\text{Q}^2(0\text{Al})$ . Given that there is a close correspondence between peak positions in the spectra of fluor-edenite and pargasite, it seems reasonable to use the fluor-edenite spectrum to assign pargasite peaks. On this basis the intensity of the  $\text{Q}^2(0\text{Al})$  peak at  $-86$  ppm, calculated from the  $\text{Q}^2(1\text{Al})$  peak at  $-82$  ppm, is 14% for pargasite. Conversely, we can use Equation 4 to calculate the  $\text{Q}^2(1\text{Al})$  peak intensity from the observed intensity of the  $\text{Q}^2(0\text{Al})$  peak at  $-86$  ppm. This gives a calculated  $\text{Q}^2(1\text{Al})$  peak intensity of 29% and implies that about 12% of the intensity of the  $-82$  ppm peak is unassigned. Given that the presence of  $\text{Q}^3(0\text{Al})$  groupings in pargasite (the  $-89$  ppm peak) implies some long-range disorder and the presence of  $\text{Q}^3(2\text{Al})$  groupings (Fig. 2), the residual intensity may be due to an unresolved  $\text{Q}^3(2\text{Al})$  peak associated with the major  $\text{Q}^2(1\text{Al})$  peak at  $-82$  ppm. It is possible to obtain a six-peak simulation of the pargasite spectrum in which the  $-82$  ppm peak is treated as an unresolved pair of peaks at  $-81.7$  ppm [ $\text{Q}^2(1\text{Al})$ ] and  $-83.1$  ppm [ $\text{Q}^3(2\text{Al})$ ] with relative intensities of 30–31% and 10–11%, respectively. This does not change the intensities of the other four peaks. In passing we note that chlorites and trioctahedral micas also have  $\delta$   $\text{Q}^3(2\text{Al}) \approx -83$  ppm (Circone et al. 1991; Welch et al. 1995). The calculated intensities of the  $\text{Q}^2(1\text{Al})$  and  $\text{Q}^2(0\text{Al})$  peaks for the six-peak simulation agree well with their simulated intensities (Table 3). To reconcile completely the  $\text{Q}^2(1\text{Al})$  and  $\text{Q}^2(0\text{Al})$  calculated intensities with each other and with their simulated intensities we have taken  $\text{Q}^2(0\text{Al}) = 19 \pm 1\%$  and  $\text{Q}^2(1\text{Al}) = 29 \pm 2\%$ . This is acceptable for the small absolute errors on peak intensities arising from the simulation (1%). From this assumption we obtain a value of  $\Psi = 0.45 \pm 0.1$ , which corresponds to  $0.55 \pm 0.1$  Al apfu at T2 and implies that the pargasite has considerable long-range disorder. The  $\text{Q}^3$  sum of 39–40% (Table 3) is consistent with about 40% long-range disorder. It appears that this is the only inter-

pretation compatible with the peak assignments for the fluor-edenite spectrum (which are well-founded) and the discrepancy between the calculated and observed intensities for the  $Q^2(OAl)$  peak at  $-86$  ppm, which arises from treating the  $-82$  ppm  $Q^2(1Al)$  as a single (over-intense) peak. Furthermore, assigning the  $-84.5$  ppm peak in the pargasite spectrum to  $Q^2(OAl)$  contradicts the observed very minor dependence of  $\delta Q^2(OAl)$  upon the A cation (Table 2) and the otherwise excellent correlation between peak positions in the fluor-edenite and pargasite spectra. Because this is clearly a complex issue, we only wish to emphasize that some, possibly considerable, long-range Al-Si disorder in pargasite is implied by the presence of an unequivocal  $Q^3(OAl)$  peak at  $-89.0$  ppm.

#### Bond-valence constraints on Al-Si long-range ordering

For comprehensive descriptions of the bond-valence method refer to Brown and Shannon (1973), Brown (1981), and Hawthorne (1992), and for its application to cation ordering in amphiboles to Hawthorne (1983, 1997). Following these authors, we distinguish between Pauling bond strength and bond valence. The first is simply the formal valence of an ion divided by its coordination number, and it relates to Pauling's second rule: The sum of the bond strengths at each atom is equal to the magnitude of the atomic valence. Bond valence as used here refers specifically to the empirical relations between bond length and bond strength parameterized by Brown and Shannon (1973) in which deviations from Pauling bond strengths for many cation-anion pairs are quantified and correlated with bond length using a database of hundreds of determined structures. The valence-sum rule states that (ideally): The sum of the bond valences at each atom is equal to the magnitude of the atomic valence; this is the so-called valence-matching principle (Hawthorne 1992). When interatomic distances are known, then the bond valences can be calculated from the curves of Brown and Shannon (1973) and Brown (1981). However deviations from the valence-sum rule do occur and prediction of likely long- and short-range order schemes using the bond-valence method relies upon the observation that, within limits, these deviations can be accommodated by structural distortion. As pointed out by Hawthorne (1997), one cannot give a meaningful universal limiting value for the size of the deviation from the valence-sum rule that is applicable to all structures—the limiting values are structure-dependent. For a given structure there is a range of deviations from the valence-sum rule that is characteristic of that structure, and configurations having bond valence sums outside these limits should not, on bond valence grounds, occur. Those inside the limits can be accommodated by structural distortion. For the amphibole structure, O at O4 has bond-valence sums ranging from 1.80–1.90 v.u., whereas the bond-valence sums of other anions are 1.85–2.15 v.u. These values can be used to set tentative bond-valence limits upon the likelihood of different cation configurations around anions in amphiboles.

The principal bond-valence constraint upon long-range Al-Si ordering in amphiboles is due to O4. This O atom is threefold-coordinated and bonded to the T2, M2, and M4 sites (Fig. 1). It is the most underbonded O atom in the amphibole structure (bond-valence sum  $\sim 1.80$ – $1.90$  v.u.). Tremolite (T2 = Si, M2 = Mg, M4 = Ca) has an O4 Pauling bond-strength sum of 1.58 v.u. ( $1.00 + 0.33 + 0.25$ ). The structure responds by shortening O4 bonds, and the resulting O4 bond-valence sum is 1.84 v.u. (Hawthorne 1997). If Al replaces Si at T2, the bond-strength sum is only 1.33 v.u. ( $0.75 + 0.33 + 0.25$ ). However, if there is also Al at M2 the O4 bond-strength sum is 1.5 v.u. ( $0.75 + 0.50 + 0.25$ ). At high temperatures a structure may tolerate bigger deviations from Pauling's second rule than it can at low or moderate temperatures, by being able to distort more and achieve acceptable bond-valence sums. Physically such relaxation in response to atomic order-disorder involves local distortions of the structure around the anions in question and may be selective, being easier for some anions than others. The tremolite structure can distort sufficiently around O4 to raise its low bond-strength sum of 1.58 v.u. to an acceptable bond-valence sum of 1.84 v.u. Does this also occur for the  $^{T2}Al^{M2}Al^{M4}Ca$  configuration (1.5  $\rightarrow$  1.8 v.u.) in pargasite and magnesiohornblende?

Hawthorne (1997) performed bond-valence calculations for different long- and short-range cation ordering schemes in calcic, sodic-calcic, and alkali amphiboles. He found that for pargasite and magnesiohornblende any configurations with Al at T2 were, on bond-valence grounds, unlikely to occur. Why then does NMR spectroscopy point to some (possibly considerable) long-range Al-Si disorder in these high-temperature synthetic amphiboles? Although it appears to be the case that  $^{41}Al$  is highly ordered at T1 in many amphiboles, Oberti et al. (1995a) found that some high-temperature natural amphiboles have up to 25% of  $^{41}Al$  at T2 ( $\Psi = 0.5$ ) and up to 0.43 Al apfu at T2. Evidently at high temperatures the structures of these  $^{41}Al$ -bearing amphiboles can distort locally around O4 and achieve an acceptable bond-valence sum. On the other hand, fluor-edenite, with only Mg on octahedral sites, has too low an O4 bond-strength sum ( $0.75 + 0.33 + 0.25 = 1.33$  v.u.) to allow Al into T2. The amphibole structure can, at high temperatures, accommodate an O4 bond-strength sum of 1.5 v.u. An O4 bond-strength sum of 1.33 v.u. is too low to be accommodated, even at 1000 °C (fluor-edenite). Hawthorne (1997) suggested a possible coupling between Al at M2 and T1 through the more favorable O1 bond-valence sum that results when Al rather than Si is at T1. Interestingly, Jenkins (1994) found that the activity-composition relation of synthetic tremolite-tschermakite amphiboles most compatible with his experimental phase-equilibrium data involved coupling between Al at M2 and T1. Notions of  $^{M2}Al$ - $^{T1}Al$  coupling on the basis of bond-valence considerations can, therefore, have real physical significance. We propose that  $^{M2}Al$ - $^{T2}Al$  coupling is important in con-

trolling Al-Si long-range disorder in pargasite and hornblendes.

### Comparisons with X-ray diffraction studies of Al-Si order-disorder

In their X-ray study of Al-Si order-disorder, Oberti et al. (1995a) found a significant temperature dependence for the mean T1-O and T2-O bond lengths in igneous pargasitic amphiboles at  $\sim 800$  °C and above, implying that temperature-dependent Al-Si long-range disorder occurs. Our calculated  $\Psi$  value of  $0.45 \pm 0.1$  for pargasite derived from the NMR data agrees well with an extrapolation of the trends defined by these workers for natural amphiboles to  $^{41}\text{Al} = 2$  apfu at 900 °C. It is also consistent with that observed by Jenkins and Hawthorne (1995) for the most Ga<sup>3+</sup>-rich tremolite-pargasite (their Parg 6–4) for which  $\Psi = 0.5 \pm 0.1$  ( $^{72}\text{Ga} = 0.42 \pm 0.09$  apfu) at 1000 °C, as determined by Rietveld refinement of XRD powder data. Thus, the natural and synthetic amphiboles appear to show similar Al-Si order-disorder behavior.

### ACKNOWLEDGMENTS

We thank the Natural History Museum (London) for a Senior Research Fellowship to M.D.W. S.L. was funded by a Sino-British Friendship Scholarship Scheme. We are grateful to Colin Graham, Steve Elphick, and NERC for access to the high-pressure facilities at the Department of Geology and Geophysics, Edinburgh University. Brian Phillips is thanked for his helpful comments on an earlier version of this paper. Part of this study was funded by NERC grant GR9/02634 to M.D.W.

### REFERENCES CITED

- Boschmann, K., Burns, P.C., Hawthorne, F.C., Raudsepp, M., and Turnock, A.C. (1994) A site disorder in synthetic fluor-edenite, a crystal structure study. *Canadian Mineralogist*, 32, 21–30.
- Brown, I.D. (1981) The bond-valence method: An empirical approach to chemical structure and bonding. In M. O'Keeffe and A. Navrotsky, Eds., *Structure and bonding in crystals*, vol. 2, p. 1–30. Academic Press, New York.
- Brown, I.D. and Shannon, R.D. (1973) Empirical bond-strength-bond-length curves for oxides. *Acta Crystallographica*, A29, 266–282.
- Circone, S., Navrotsky, A., Kirkpatrick, R.J., and Graham, C.M. (1991) Substitution of  $^{64}\text{Al}$  in phlogopite: Mica characterization, unit-cell variation,  $^{27}\text{Al}$  and  $^{29}\text{Si}$  MAS NMR spectroscopy, and Al-Si distribution in the tetrahedral sheet. *American Mineralogist*, 76, 1485–1501.
- Della Ventura, G. and Robert, J-L. (1990) Synthesis, XRD and FTIR studies of strontium richterites. *European Journal of Mineralogy*, 2, 171–175.
- Della Ventura, G., Robert, J-L., Bény, J-M., Raudsepp, M., and Hawthorne, F.C. (1993a) The OH-F substitution in Ti-rich potassium richterite: Rietveld structure refinement and FTIR and micro-Raman spectroscopic studies of synthetic amphiboles in the system  $\text{K}_2\text{O-Na}_2\text{O-CaO-MgO-SiO}_2\text{-TiO}_2\text{-H}_2\text{O-HF}$ . *American Mineralogist*, 78, 980–987.
- Della Ventura, G., Robert, J-L., Raudsepp, M., and Hawthorne, F.C. (1993b) Site occupancies in monoclinic amphiboles: Rietveld structure refinement of synthetic nickel magnesium cobalt potassium richterite. *American Mineralogist*, 78, 633–640.
- Della Ventura, G., Robert, J-L., Raudsepp, M., Hawthorne, F.C., and Welch, M.D. (1997) Site occupancies in synthetic monoclinic amphiboles: Rietveld structure refinement and infrared spectroscopy of (nickel, magnesium, cobalt)-richterite. *American Mineralogist*, 82, 291–301.
- Graham, C.M. and Navrotsky, A. (1986) Thermochemistry of the tremolite-edenite amphiboles using fluorine analogues, and applications to amphibole-plagioclase-quartz equilibria. *Contributions to Mineralogy and Petrology*, 93, 18–32.
- Hamilton, D.L. and Henderson, C.M.B. (1968) The preparation of silicate compositions by a gelling method. *Mineralogical Magazine*, 36, 832–838.
- Hawthorne, F.C. (1983) The crystal chemistry of the amphiboles: Polyvalent-cation ordering in clinoamphiboles. *Canadian Mineralogist*, 21, 173–480.
- (1992) Bond topology, bond valence, and structure stability. In G.D. Price and N.L. Ross, Eds., *The stability of minerals. The Mineralogical Society of Great Britain and Ireland, Series 3*, 25–87.
- (1995) A multinuclear NMR study of synthetic pargasite—Discussion. *American Mineralogist*, 80, 628–629.
- (1997) Short-range order in amphiboles: A bond-valence approach. *Canadian Mineralogist*, 35, 201–216.
- Hawthorne, F.C., Della Ventura, G., and Robert, J-L. (1996a) Short-range order and long-range order in amphiboles: A model for the interpretation of the infrared spectra in the principal OH-stretching region. In M.D. Dyer, C. McCammon, and M.W. Scafer, Eds., *Mineral spectroscopy: A tribute to Roger G. Burns*, p. 49–54. The Geochemical Society, Texas.
- Hawthorne, F.C., Oberti, R., Ungaretti, L., and Grice, J.D. (1996b) A new hyper-calcic amphibole with Ca at the A site: Fluor-cannilloite from Pargas, Finland. *American Mineralogist*, 81, 995–1002.
- Hawthorne, F.C., Oberti, R., and Sardone, N. (1996c) Sodium at the A site in clinoamphiboles: The effects of composition on patterns of order. *Canadian Mineralogist*, 34, 577–593.
- Herrero, C.P., Sanz, J., and Serratos, J.M. (1985) Si, Al distribution in micas: Analysis by high-resolution  $^{29}\text{Si}$  Nmr spectroscopy. *Journal of Physics C: Solid State Physics*, 18, 13–22.
- Herrero, C.P., Gregorkiewitz, M., Sanz, J., and Serratos, J.M. (1987)  $^{29}\text{Si}$  MAS NMR spectroscopy of mica-type silicates: Observed and predicted distribution of tetrahedral Al-Si. *Physics and Chemistry of Minerals*, 15, 84–90.
- Jenkins, D.M. (1988) Experimental study of the join tremolite-tschermakite: A reinvestigation. *Contributions to Mineralogy and Petrology*, 99, 392–400.
- (1994) Experimental reversal of the aluminum content in tremolitic amphiboles in the system  $\text{H}_2\text{O-CaO-MgO-Al}_2\text{O}_3\text{-SiO}_2$ . *American Journal of Science*, 294, 593–620.
- Jenkins, D.M. and Hawthorne, F.C. (1995) Synthesis and Rietveld refinement of amphibole along the join  $\text{Ca}_2\text{Mg}_3\text{Si}_8\text{O}_{22}\text{F}_2\text{-NaCa}_2\text{Mg}_4\text{Ga}_3\text{Si}_6\text{O}_{22}\text{F}_2$ . *Canadian Mineralogist*, 33, 13–24.
- Jenkins, D.M., Sherriff, B.L., Cramer, J., and Xu, Z. (1997) Al, Si, and Mg occupancies in tetrahedrally and octahedrally coordinated sites in synthetic aluminous tremolite. *American Mineralogist*, 82, 280–290.
- Liu, S., Welch, M.D., Klinowski, J., and Maresch, W.V. (1996) A MAS NMR study of a monoclinic/triclinic phase transition in an amphibole with excess OH:  $\text{Na}_3\text{Mg}_3\text{Si}_8\text{O}_{21}(\text{OH})_3$ . *European Journal of Mineralogy*, 33, 223–229.
- Na, K.C., McCauley, M.L., Crisp, J.A., and Ernst, W.G. (1986) Amphibole stability relations in the system edenite and edenite + excess quartz +  $\text{H}_2\text{O}$ . *Lithos*, 19, 153–163.
- Oberti, R., Ungaretti, L., Canillo, E., Hawthorne, F.C., and Memmi, I. (1995a) Temperature-dependent Al order-disorder in the tetrahedral double chain of *C2/m* amphiboles. *European Journal of Mineralogy*, 7, 1049–1063.
- Oberti, R., Sardone, N., Hawthorne, F.C., Raudsepp, M., and Turnock, A.C. (1995b) Synthesis and crystal-structure refinement of synthetic fluor-pargasite. *Canadian Mineralogist*, 33, 25–31.
- Pawley, A.R. (1992) Experimental study of the compositions and stabilities of synthetic nyböite and nyböite-glaucophane amphiboles. *European Journal of Mineralogy*, 4, 171–192.
- Raudsepp, M., Turnock, A.C., Hawthorne, F.C., Sherriff, B.L., and Hartman, J.S. (1987) Characterization of synthetic pargasitic amphiboles ( $\text{NaCa}_2\text{Mg}_3\text{M}^{3+}\text{Si}_6\text{Al}_2\text{O}_{22}(\text{OH},\text{F})_2$ ;  $\text{M}^{3+} = \text{Al, Cr, Ga, Sc, In}$ ) by infrared spectroscopy, Rietveld structure refinement, and  $^{27}\text{Al}$ ,  $^{29}\text{Si}$ , and  $^{19}\text{F}$  MAS NMR spectroscopy. *American Mineralogist*, 72, 580–593.
- Robert, J-L., Della-Ventura, G.D., and Thauvin, J-L. (1989) The infrared OH-stretching region of synthetic richterites in the system  $\text{Na}_2\text{O-K}_2\text{O-CaO-MgO-SiO}_2\text{-H}_2\text{O-HF}$ . *European Journal of Mineralogy*, 1, 203–211.
- Welch, M.D. (1987) Experimental studies of selected amphiboles in the

- system  $\text{Na}_2\text{O-CaO-MgO-Al}_2\text{O}_3\text{-SiO}_2\text{-H}_2\text{O-SiF}_4$  and its subsystems. PhD thesis, University of Edinburgh, U.K.
- Welch, M.D. and Graham, C.M. (1992) An experimental study of glaucophanic amphiboles in the system  $\text{Na}_2\text{O-MgO-Al}_2\text{O}_3\text{-SiO}_2\text{-SiF}_4$  (NMAF): Some implications for glaucophane stability in natural and synthetic systems at high temperatures and pressures. *Contributions to Mineralogy and Petrology*, 111, 248–259.
- Welch, M.D. and Pawley, A.R. (1991) Tremolite: New enthalpy and entropy data from a phase equilibrium study of the reaction tremolite = 2 diopside + 1.5 orthoenstatite +  $\beta$ -Quartz +  $\text{H}_2\text{O}$ . *American Mineralogist*, 76, 1931–1939.
- Welch, M.D., Kolodziejewski, W., and Klinowski, J. (1994) A multinuclear NMR study of synthetic pargasite. *American Mineralogist*, 79, 261–268.
- Welch, M.D., Barras, J., and Klinowski, J. (1995) A multinuclear NMR study of clinocllore. *American Mineralogist*, 80, 441–447.

MANUSCRIPT RECEIVED APRIL 14, 1997

MANUSCRIPT ACCEPTED AUGUST 19, 1997